Copyright © 2009 Tech Science Press CMES, vol.39, no.3, pp.263-299, 2009

A Discontinuous Galerkin Finite Element Method for Heat Conduction Problems with Local High Gradient and Thermal Contact Resistance

Donghuan Liu[1], **Xiaoping Zheng**[1,2] **and Yinghua Liu**[1]

Abstract: A discontinuous Galerkin (DG) finite element method for the heat conduction problems with local high gradient and thermal contact resistance is presented. The DG formulation is constructed by employing the stabilization term and the Bassi-Rebay numerical flux term. The stabilization term is defined by a penalization of the temperature jump at the interface. By eliminating the penalization term of the temperature jump in the region of local high gradient and imperfect contact interfaces, the present DG method is applied to solve problems involving local high gradient and thermal contact resistance where the numerical flux is obtained from the definition of the thermal contact resistance. This treatment leads to a novel approach to capture the peak value of the heat flux in local high gradient field and the temperature jump at the imperfect contact interface. Moreover, an iterative procedure and a relaxation technique are also adopted herein to simulate the nonlinear thermoelastic coupling between thermal contact resistance, temperature and stress field, which can easily avoid numerical instability and gets reasonable results.

Several numerical examples are given to demonstrate the accuracy and the reliability of the present DG finite element method. From our investigations, we find that the DG method is an attractive and competitive approach for solving heat conduction problems with local high gradient and thermal contact resistance, and also can easily avoid numerically instability in dealing with nonlinear coupling problems caused by thermal contact resistance.

Keywords: discontinuous Galerkin method, thermal contact resistance, high gradient, thermoelastic coupling, heat conduction problem

[1] Department of Engineering Mechanics, FML, Tsinghua University, Beijing 100084, P.R. China

[2] Corresponding author, Tel: 86-10-62796187; fax: 86-10-62781824; Email: zhengxp@mail.tsinghua.edu.cn

1 Introduction

Interest in heat conduction problems with local high gradient and thermal contact resistance originally received a strong impulse from nuclear, aeronautic and aerospace technologies. In problems such as nuclear reactors, layered structures, heat exchangers and heat removal from electronic devices, thermal contact resistance plays a very important role [Bahrami et al. (2006)]. In the high gradient temperature field problems, even with a very refined mesh, it is difficult to capture the peak value of the heat flux by using traditional continuous Galerkin finite element method, unless it is coupled with some special techniques such as curvilinear spectral overlay method [Belytschko and Lu (1992)]. In order to simulate the temperature discontinuity phenomenon at the contact interface caused by thermal contact resistance, the continuous Galerkin method employs interface elements to perform the analyses [Blandford and Tauchert (1985)], and this approach introduces additional freedom at the interface. Some researchers employ mesheless local Petrov-Galerkin (MLPG) method [Li et al. (2003)], or the moving least squares (MLS) approximation scheme of element-free Galerkin (EFG) method [Masuda and Noguchi (2006)], or the boundary element method [Keppas et al. (2008)], or the Material Point Method (MPM) [Chen et al. (2008)], to model other discontinuous phenomena such as material discontinuity on the interface.

Since the discontinuous Galerkin (DG) finite element method allows discontinuities of the physical unknowns within the interior of the problem domain, it seems to be a natural approach to capture these discontinuities numerically. This DG methodology results from the integration by parts on the finite element of the governing equations multiplied by discontinuous weighting functions. Physical unknowns and weighting functions are substituted by a discontinuous polynomial approximation respectively. Since this integration by parts is applied to finite element, it leads to element boundary integral terms usually referred to as numerical fluxes. These terms enforce the consistency and the continuity of the problem unknowns in a weak manner.

The first DG method was introduced by Reed and Hill for the neutron transport equation [Reed and Hill (1973)], which is a linear hyperbolic partial differential equation. Due to the properties of locally conservative, high-order accurate, and dissipation or stabilization through jumps in the DG method, even in convection-dominated regimes, the DG method has received considerable attention in computational fluid dynamics, for example, in gas dynamics [Bassi and Rebay (1997)], compressible [Bassi and Rebay (1997)] and incompressible [Cockburn et al. (2005)] flows, magneto-hydrodynamics [Warburton and Karniadakis (1999)], and other fields, like structural dynamics [Li and Wiberg (1998); Chien and Wu (2008)], modeling of functionally graded and layered materials [Aksoy and Senocak (2005)],

Maxwell equations [Dolean et al. (2008)], et al.

Although the original impetus of most researches on the DG method was the solution of hyperbolic and parabolic problems, the applications of the DG method have also spread to the elliptic problems [Arnold et al. (2002)]. Some representative examples are Timoshenko beams [Celiker et al. (2006)], shells [G uzey et al. (2006); G uzey et al. (2007)], nonlinear elasticity [Eyck and Lew (2006)], hyperelasticity [Noels and Radovitzky (2006)], incompressible and nearly incompressible linear elasticity [Hansbo and Larson (2002)], strain gradient elasticity [Engel et al. (2002)], elastoplasticity [Alberty and Carstensen (2002)], et al. Khalmanova and Costanzo proposed a space-time discontinuous Galerkin finite element method for fully coupled linear thermo-elasto-dynamic problems with strain and heat flux discontinuities [Khalmanova and Costanzo (2008)], but they didn't consider the discontinuity caused by the imperfect contact on the material interface. Kanapady, et al. provided the so-called local discontinuous Galerkin (LDG) method for solving various kinds of heat conduction problems with temperature discontinuity caused by thermal contact resistance [Kanapady et al. (2005); Jain et al. (2006)]. For a detailed overview of the DG method, from the theoretical, performance and application perspectives we refer the readers to the review articles [Cockburn et al. (2000); Cockburn (2003)] and the references therein. However, up to now, to the authors' knowledge, the application of the DG method on the heat conduction problems with local high gradient and thermal contact resistance has not been met.

The main purpose of this paper is to develop the DG finite element method to solve heat conduction problems with local high gradient and thermal contact resistance where the DG concept can show its advantages compared to the continuous formulation. The present DG method is also extended to solve the nonlinear coupling problems caused by thermal contact resistance.

The paper is organized as follows: Section 2 provides the detailed formulation and implementation of the DG finite element method for heat conduction problems. Section 3 presents examples provides several numerical evidences and applications in engineering problems of the established properties of the DG finite element method. Finally, some conclusions and discussions are given in Section 4.

2 Formulation of the DG finite element method

In this section, we introduce the formulation of the DG finite element method as applied to the equations of heat conduction problems.

2.1 Problem definition

We consider the following heat conduction problem on the domain Ω bounded by $\partial\Omega$, as shown in Fig. 1. The governing equations can be expressed as:

$$\nabla \cdot \mathbf{q} - f = 0 \quad \text{on } \Omega \tag{1}$$

$$\mathbf{q} + \mathbf{k}(\mathbf{x})\Delta T = 0 \quad \text{on } \Omega \tag{2}$$

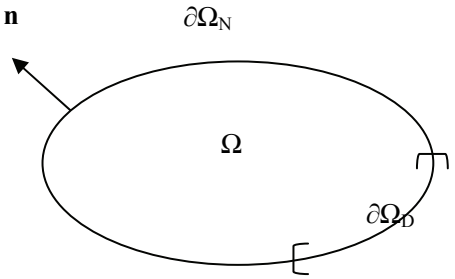

Figure 1: Solution domain and its boundary parts. $\partial\Omega_D$ and $\partial\Omega_N$ represent the parts of the boundary where Dirichlet and Neumann boundary conditions, respectively, are applied

The boundary $\partial\Omega$ is decomposed into a region of Dirichlet boundary conditions $\partial\Omega_D$ and Neumann boundary conditions $\partial\Omega_N$ (i.e. $\partial\Omega_D \cup \partial\Omega_N = \partial\Omega$ and $\partial\Omega_D \cap \partial\Omega_N = \emptyset$):

$$T = \bar{T} \quad \text{on } \partial\Omega_D \tag{3}$$

$$\mathbf{n} \cdot \mathbf{q} = \bar{\mathbf{q}} \quad \text{on } \partial\Omega_N \tag{4}$$

In Equations (1)-(4), ∇ denotes the gradient operator, $\mathbf{q}$ is the heat flux, f is the heat source, $\mathbf{k}(\mathbf{x})$ is a symmetric matrix of thermal conductivity coefficients which may vary in space, T is the temperature field, $\bar{T}$ and $\bar{\mathbf{q}}$ are the prescribed temperature and heat flux respectively, $\mathbf{n}$ is the outward unit normal to the boundary $\partial\Omega$.

Equations (1)-(4) are the governing differential equation for the heat conduction problem, which are also called strong form of the problem. The solution for the strong form must satisfy the differential Equations (1) and (2) at each point of the domain and the boundary conditions (3) and (4). In order to obtain the approximate solution of the problem, by taking the inner product of Equations (1) and (2) with

weighting functions v and $\mathbf{w}$ respectively, over the solution domain Ω we obtain the weak form of the problem:

$$\int_{\Omega} v\,(\nabla\cdot\mathbf{q}-f)\,\mathrm{d}\Omega = 0 \quad \text{on } \Omega \tag{5}$$

$$\int_{\Omega} \mathbf{w}\cdot(\mathbf{q}+\mathbf{k}\nabla T)\,\mathrm{d}\Omega = 0 \quad \text{on } \Omega \tag{6}$$

where weighting functions v and $\mathbf{w}$ are a set of arbitrary functions equal in number to the number of equations involved.

2.2 Elemental formulation of the weak form

For a two dimensional problem we assume $\Im(\Omega)$ is a two dimensional tessellation of the domain Ω. Let $\Omega^e \in \Im(\Omega)$ bounded by $\partial\Omega^e$ be a non-overlapping element within the tessellation such that if $e_1 \neq e_2$ then $\Omega^{e_1} \cap \Omega^{e_2} = \emptyset$, and it may have hanging nodes and elements of various shapes. We define the following two spaces for our discontinuous approximations:

$$V_h := \left\{ v \in L^2(\Omega) : v|_{\Omega^e} \in P(\Omega^e)\,\forall\Omega^e \in \Im \right\}$$
$$\Sigma_h := \left\{ \mathbf{w} \in \left(L^2(\Omega)\right)^2 : \mathbf{w}|_{\Omega^e} \in \Sigma(\Omega^e)\,\forall\Omega^e \in \Im \right\}$$

where $P(\Omega^e)$ is the space of linear polynomial functions and $\Sigma(\Omega^e) = (P(\Omega^e))^2$. We assume that the discrete spaces, V_h and Σ_h, are finite dimensional. Fig. 2 illustrates the discontinuous nature of the approximation functions across interior element boundaries for a three elements patch of linear triangles.

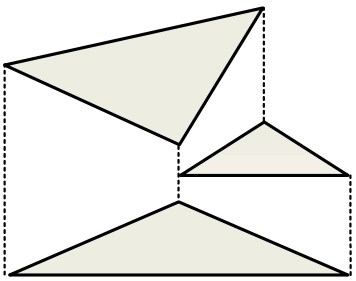

Figure 2: Illustration of approximation functions for the DG method on a three element patch of linear triangles

Let $v^e \in V_h$ and $\mathbf{w}^e \in \Sigma_h$ denote the scalar and vector weighting functions respectively, defined on an element Ω^e. Now the problem reduces to finding $T^e \in V_h$ and

$\mathbf{q}^e \in \Sigma_h$ such that for all $\Omega^e \in \Im(\Omega)$ we have:

$$\int_{\Omega^e} v^e (\nabla \cdot \mathbf{q}^e - f^e) \, \mathrm{d}\Omega = 0 \quad \forall v^e \in V_h \tag{7}$$

$$\int_{\Omega^e} \mathbf{w}^e \cdot (\mathbf{q}^e + \mathbf{K}^e \nabla T^e) \, \mathrm{d}\Omega = 0 \quad \forall \mathbf{w}^e \in \Sigma_h \tag{8}$$

Integrating by parts the terms associated with the divergence in Equation (7) and gradient in Equation (8) lead to:

$$\int_{\Omega^e} v^e \nabla \cdot \mathbf{q}^e \mathrm{d}\Omega = \oint_{\partial\Omega^e} v^e (\mathbf{n}^e \cdot \mathbf{q}^e) \, \mathrm{d}\Gamma - \int_{\Omega^e} \nabla v^e \cdot \mathbf{q}^e \mathrm{d}\Omega \tag{9}$$

$$\int_{\Omega^e} \mathbf{w}^e \cdot (\mathbf{K}^e \nabla T^e) \, \mathrm{d}\Omega = \oint_{\partial\Omega^e} T^e (\mathbf{K}^e \mathbf{w}^e) \cdot \mathbf{n}^e \mathrm{d}\Gamma - \int_{\Omega^e} T^e \nabla \cdot (\mathbf{K}^e \mathbf{w}^e) \, \mathrm{d}\Omega \tag{10}$$

where $\mathbf{n}^e$ is the outward unit normal to the boundary $\partial\Omega^e$.

Substituting Equation (9) into Equation (7) and substituting Equation (10) into Equation (8), the following form can be obtained:

$$\int_{\Omega^e} (\nabla v^e \cdot \mathbf{q}^e + v^e f^e) \, \mathrm{d}\Omega = \oint_{\partial\Omega^e} v^e (\mathbf{n}^e \cdot \mathbf{q}^e) \, \mathrm{d}\Gamma \tag{11}$$

$$\int_{\Omega^e} (T^e \nabla \cdot (\mathbf{K}^e \mathbf{w}^e) - \mathbf{w}^e \cdot \mathbf{q}^e) \, \mathrm{d}\Omega = \oint_{\partial\Omega^e} T^e (\mathbf{K}^e \mathbf{w}^e) \cdot \mathbf{n}^e \mathrm{d}\Gamma \tag{12}$$

In Equations (11) and (12) we note that the values of $\mathbf{q}^e$ and T^e are required in the boundary integration terms $\oint_{\partial\Omega^e} v^e (\mathbf{n}^e \cdot \mathbf{q}^e) \, \mathrm{d}\Gamma$ and $\oint_{\partial\Omega^e} T^e (\mathbf{K}^e \mathbf{w}^e) \cdot \mathbf{n}^e \mathrm{d}\Gamma$ of each element respectively. Since the main feature of the traditional continuous Galerkin finite element method is the assumption of continuity in the primary variable across interior boundaries, after the global assembly procedure the internal boundary integration terms disappeared. But due to the discontinuous nature of the approximation functions in the DG finite element, interelement discontinuity is allowed, so in the DG formulation continuity of the unknown variables are enforced by using stabilization terms and numerical fluxes between the interior elemental boundaries which will be discussed in the following subsections. Finally, we must note that in the above discussion it was implicitly assumed that all the integrals are capable of being evaluated.

2.2.1 Numerical flux

In the present DG formulation, we replace the element heat flux $\mathbf{q}^e$ and element temperature T^e in the boundary integration terms by the so-called numerical fluxes $\hat{\mathbf{q}}^e$ and $\hat{T}^e$ respectively to obtain the DG finite element equations:

$$\int_{\Omega^e} (\nabla v^e \cdot \mathbf{q}^e + v^e f^e) \, \mathrm{d}\Omega = \oint_{\partial\Omega^e} v^e (\mathbf{n}^e \cdot \hat{\mathbf{q}}^e) \, \mathrm{d}\Gamma \tag{13}$$

$$\int_{\Omega^e} \left(T^e \nabla \cdot (\mathbf{K}^e \mathbf{w}^e) - \mathbf{w}^e \cdot \mathbf{q}^e\right) \mathrm{d}\Omega = \oint_{\partial\Omega^e} \hat{T}^e \left(\mathbf{K}^e \mathbf{w}^e\right) \cdot \mathbf{n}^e \mathrm{d}\Gamma \tag{14}$$

The temperature numerical flux $\hat{T}^e$ can be expressed in terms of T^e and T^{eb}, and heat flux numerical flux $\hat{\mathbf{q}}^e$ can be expressed in terms of $\mathbf{q}^e$ and $\mathbf{q}^{eb}$, where T^{eb} and $\mathbf{q}^{eb}$ denote the temperature and heat flux in the element eb , respectively. Here the superscript "eb" denotes the neighbor element of element e. The choice of the numerical fluxes is quite delicate, as it has great effect on the stability and accuracy of the method as well as the sparsity and symmetry of the stiffness matrix.

In the present research the numerical fluxes at the interior boundary Γ^{eb} of element e neighbored with element eb are defined by:

$$\hat{T}^e = \alpha_T T^e + \beta_T T^{eb} \text{ on } \Gamma^{eb} \tag{15}$$

$$\hat{\mathbf{q}}^e = \alpha_q \mathbf{q}^e + \beta_q \mathbf{q}^{eb} \text{ on } \Gamma^{eb} \tag{16}$$

From a consistency point of view, the real valued numerical flux coefficients α_T, β_T, α_q and β_q should satisfy the constraint:

$$\begin{aligned} \alpha_T + \beta_T &= 1 \\ \alpha_q + \beta_q &= 1 \end{aligned} \tag{17}$$

We can get different versions of DG finite element methodology by using different numerical flux coefficients. A simple and natural choice of the numerical fluxes is proposed by Bassi and Rebay [Bassi and Rebay (1997)], which is so-called the Bassi-Rebay numerical fluxes. It takes the arithmetic average of the two values of temperature T and heat flux $\mathbf{q}$ at the boundary of the elements as the numerical fluxes $\hat{T}^e$ and $\hat{q}^e$ respectively:

$$\hat{T}^e = \frac{1}{2}\left(T^e + T^{eb}\right) \text{ on } \Gamma^{eb} \tag{18}$$

$$\hat{\mathbf{q}}^e = \frac{1}{2}\left(\mathbf{q}^e + \mathbf{q}^{eb}\right) \text{ on } \Gamma^{eb} \tag{19}$$

Numerical fluxes (18) and (19) implies that $\alpha_T = \beta_T = \alpha_q = \beta_q = 1/2$.

If part of the element boundary $\partial\Omega^{ext} \in (\partial\Omega_D \cup \partial\Omega_N)$, then the numerical fluxes on the external boundary $\partial\Omega^{ext}$ are defined by:

$$\hat{T}^e = \begin{cases} \bar{T} & \text{if } \partial\Omega^{ext} \in \partial\Omega_D \\ T^e & \text{if } \partial\Omega^{ext} \in \partial\Omega_N \end{cases} \tag{20}$$

$$\mathbf{n}^e \cdot \hat{\mathbf{q}}^e = \begin{cases} \bar{q} & \text{if } \partial\Omega^{ext} \in \partial\Omega_N \\ \mathbf{n}^e \cdot \mathbf{q}^e & \text{if } \partial\Omega^{ext} \in \partial\Omega_D \end{cases} \tag{21}$$

2.2.2 Stabilization

The stabilization terms in the formulation of DG method are of crucial importance. Brezzi et al. investigated the stabilization mechanisms in DG methods [Brezzi et al. (2006)]. Sherwin et al. pointed out that stabilization is necessary when using the Bassi-Rebay boundary numerical fluxes [Sherwin et al. (2006)], and it can also enhance the numerical stability and accuracy when using other kinds of numerical fluxes. Typically, stabilization can be defined as the penalization of the jump of the primitive variable at the interface of two neighbored elements $\int_{\Gamma^{eb}} \tau v^e \left(T^e - T^{eb}\right) \mathrm{d}\Gamma$, where τ is the stabilization parameter, and it can be interpreted as the weak enforcement of continuity of the primitive variable across interior boundaries. Nitsche introduced a least-squares term $\int_{\Gamma^{eb}} \tau v^e \left(T^e - T^{eb}\right)^2 \mathrm{d}\Gamma$ as the stabilization term, and he also showed that for linear element, the stabilization parameter τ should be $O\left(\|\mathbf{K}^e\|/h\right) > 0$, where h is an element size measure and $\|\mathbf{K}^e\|$ is a norm of the thermal conduction coefficient matrix [Zienkiewicz et al. (2003)].

In the present research we adopt the penalization of the jump of the temperature at the interface, so the stabilized DG finite element equations can be written as:

$$\int_{\Omega^e} \left(\nabla v^e \cdot \mathbf{q}^e + v^e f^e\right) \mathrm{d}\Omega + \sum_{eb=1}^{N_b^e} \int_{\Gamma^{eb}} \tau v^e \left(T^e - T^{eb}\right) \mathrm{d}\Gamma = \oint_{\partial\Omega^e} v^e \left(\mathbf{n}^e \cdot \hat{\mathbf{q}}^e\right) \mathrm{d}\Gamma \tag{22}$$

$$\int_{\Omega^e} \left(T^e \nabla \cdot \left(\mathbf{K}^e \mathbf{w}^e\right) - \mathbf{w}^e \cdot \mathbf{q}^e\right) \mathrm{d}\Omega = \oint_{\partial\Omega^e} \hat{T}^e \left(\mathbf{K}^e \mathbf{w}^e\right) \cdot \mathbf{n}^e \mathrm{d}\Gamma \tag{23}$$

where N_b^e denotes the number of boundary segments in element e, Γ^{eb} denotes the eb-th boundary segment in element e.

2.3 DG finite element equation

Suppose that the temperature T^e and heat flux $\mathbf{q}^e$ are approximated over a typical finite element Ω^e by the expressions:

$$T^e = \mathbf{N}_T^e \delta\mathbf{T}^e, \quad \mathbf{q}^e = \mathbf{N}_q^e \delta\mathbf{q}^e \tag{24}$$

where $\delta\mathbf{T}^e$ and $\delta\mathbf{q}^e$ denote listings of nodal temperatures and heat fluxes for element e. $\mathbf{N}_T^e$ and $\mathbf{N}_q^e$ denote the expansion basis or shape functions. Here the shape functions can be constructed independently in each element domain Ω^e , so that the order of the approximating polynomial can be easily changed from one element to the other and refinement of the grid can be achieved without taking into account the continuity restrictions which is typical of continuous finite element methods,

and this makes the DG method can easily handle adaptivity strategies. In order to obtain a Galerkin style formulation, the weighting functions v^e and $\mathbf{w}^e$ are taken as:

$$\begin{aligned} v^e &= \left(\mathbf{N}_T^e\right)^T \\ \mathbf{w}^e &= \left(\mathbf{N}_q^e\right)^T \end{aligned} \tag{25}$$

Substituting Equations (24) and (25) into Equations (22) and (23), the following DG finite element equations can be obtained:

$$\begin{aligned} &\left(\mathbf{K}_3^e - \mathbf{K}_1^e\right)\delta\mathbf{q}^e + \sum_{eb=1}^{N_b^e} \mathbf{K}_3^{eb}\delta\mathbf{q}^{eb} - \mathbf{K}_2^e\delta\mathbf{T}^e - \sum_{eb=1}^{N_b^e} \mathbf{K}_2^{eb}\delta\mathbf{T}^{eb} = \mathbf{F}_T^e \\ &\mathbf{K}_5^e\delta\mathbf{q}^e + \left(\mathbf{K}_6^e - \mathbf{K}_4^e\right)\delta\mathbf{T}^e + \sum_{eb=1}^{N_b^e} \mathbf{K}_6^{eb}\delta\mathbf{T}^{eb} = 0 \end{aligned} \tag{26}$$

where we have used the definitions described in the following.

The term $\mathbf{K}_1^e$ corresponds to the elemental contribution which is typically arises in a continuous Galerkin finite element formulation:

$$\mathbf{K}_1^e = \int_{\Omega^e} \nabla\left(\mathbf{N}_T^e\right)^T \cdot \mathbf{N}_q^e \mathrm{d}\Omega \tag{27}$$

$\mathbf{K}_2^e$ and $\mathbf{K}_2^{eb}$ denote the contribution of stabilization and are given by:

$$\begin{aligned} \mathbf{K}_2^e &= \oint_{\partial\Omega^e} \tau\left(\mathbf{N}_T^e\right)^T \mathbf{N}_T^e \mathrm{d}\Omega \\ \mathbf{K}_2^{eb} &= \int_{\Gamma^{eb}} -\tau\left(\mathbf{N}_T^e\right)^T \mathbf{N}_T^{eb} \mathrm{d}\Gamma \end{aligned} \tag{28}$$

$\mathbf{K}_3^e$ and $\mathbf{K}_3^{eb}$ denote the contribution of interface integration caused by the heat flux numerical flux $\hat{\mathbf{q}}^e$ and are given by:

$$\begin{aligned} \mathbf{K}_3^e &= \oint_{\partial\Omega^e} \alpha_q\left(\mathbf{N}_T^e\right)^T \left(\mathbf{n}^e \cdot \mathbf{N}_q^e\right) \mathrm{d}\Gamma \\ \mathbf{K}_3^{eb} &= -\int_{\Gamma^{eb}} \beta_q\left(\mathbf{N}_T^e\right)^T \left(\mathbf{n}^e \cdot \mathbf{N}_q^{eb}\right) \mathrm{d}\Gamma \end{aligned} \tag{29}$$

$\mathbf{F}_T^e$ denotes the element heat load vector relating to internal heat generation and is given by:

$$\mathbf{F}_T^e = \int_{\Omega^e} \left(\mathbf{N}_T^e\right)^T f^e \mathrm{d}\Omega \tag{30}$$

$\mathbf{K}_4^e$ and $\mathbf{K}_5^e$ corresponds to the heat conduction constitutive equation and are given by:

$$\begin{aligned}\mathbf{K}_4^e &= \int_{\Omega^e} \mathbf{N}_T^e \mathbf{K}^e \nabla \cdot (\mathbf{N}_T^e)^T \, \mathrm{d}\Omega \\ \mathbf{K}_5^e &= \int_{\Omega^e} -\left(\mathbf{N}_q^e\right)^T \mathbf{N}_q^e \mathrm{d}\Omega\end{aligned} \tag{31}$$

$\mathbf{K}_6^e$ and $\mathbf{K}_6^{eb}$ corresponds to the contribution of interface integration caused by the temperature numerical flux $\hat{T}^e$ and are given by:

$$\begin{aligned}\mathbf{K}_6^e &= \oint_{\partial\Omega^e} \alpha_T \mathbf{N}_T^e \mathbf{K}^e \left(\mathbf{N}_q^e\right)^T \cdot \mathbf{n}^e \mathrm{d}\Gamma \\ \mathbf{K}_6^{eb} &= \int_{\Gamma^{eb}} \beta_T \mathbf{N}_T^{eb} \mathbf{K}^e \left(\mathbf{N}_q^e\right)^T \cdot \mathbf{n}^e \mathrm{d}\Gamma\end{aligned} \tag{32}$$

If the temperature numerical flux $\hat{T}^e$ is independent with the heat flux on the element interior boundary, then the variable $\mathbf{q}^e$ can be solved through Equation (23) in an element-by-element fashion to get:

$$\delta\mathbf{q}^e = \left(\mathbf{K}_5^e\right)^{-1} \left(\left(\mathbf{K}_4^e - \mathbf{K}_6^e\right) \delta\mathbf{T}^e - \sum_{eb=1}^{N_b^e} \left(\mathbf{K}_6^{eb} \delta\mathbf{T}^{eb} \right) \right) \tag{33}$$

Then $\mathbf{q}^e$ can be eliminated from the equations by substituting (33) into Equation (22) to get the DG finite element equation on element domain Ω^e:

$$\mathbf{K}^e \delta\mathbf{T}^e + \sum_{eb=1}^{N_b^e} \left(\mathbf{K}^{eb} \delta\mathbf{T}^{eb} + \mathbf{K}^{ebb} \delta\mathbf{T}^{ebb} \right) = \mathbf{F}_T^e \tag{34}$$

where,

$$\begin{aligned}\mathbf{K}^e &= \left(\mathbf{K}_3^e - \mathbf{K}_1^e\right) \left(\mathbf{K}_5^e\right)^{-1} \left(\mathbf{K}_4^e - \mathbf{K}_6^e\right) - \mathbf{K}_2^e \\ \mathbf{K}^{eb} &= \mathbf{K}_3^{eb} \left(\mathbf{K}_5^e\right)^{-1} \left(\mathbf{K}_4^{eb} - \mathbf{K}_6^{eb} \right) - \left(\mathbf{K}_3^e - \mathbf{K}_1^e\right) \left(\mathbf{K}_5^e\right)^{-1} \mathbf{K}_6^{eb} - \mathbf{K}_2^{eb} \\ \mathbf{K}^{ebb} &= -\sum_{ebb=1}^{N_b^{ebb}} \left(\mathbf{K}_3^{eb} \left(\mathbf{K}_5^{eb} \right)^{-1} \mathbf{K}_6^{ebb} \right)\end{aligned} \tag{35}$$

here the superscript "*ebb*" denotes the neighbor element of element *eb*.

The assembly procedure for DG finite element method is the same as that used for continuous Galerkin finite element method, and the assembled system of equations corresponding to the unknown primary variables can be written as:

$$\mathbf{K}\mathbf{T} = \mathbf{F} \tag{36}$$

After the imposition of the boundary conditions procedure, the assembled equations can be solved by traditional techniques that are widely employed for the continuous Galerkin method, then we can use Equation (23) to compute the heat flux or other desired quantities from the primary degrees of freedom computed from Equation (36).

2.4 Remarks on numerical implementation

Here we consider the continuous Galerkin finite element implementation as a baseline, and comment on the essential modifications to obtain the DG one. DG finite element method involves contributions of the stabilization and numerical flux integration terms on interior boundaries, which require the introduction of a loop over interior boundaries in addition to the loop over all the elements. This interaction between the two-neighbored elements makes it necessary to implement a search algorithm that can detect the interface of the element and its neighbor element. In the present study, we give all the neighbor information such as neighbor elements and common sides when preparing the input gridding data.

In the following subsections, we give some remarks on the numerical implementation of the DG finite element method in solving problems involve local high gradient, imperfect thermal contact and thermoelastic coupling.

2.4.1 Problems with local high gradient

Local high gradient temperature field is usually caused by the sharp change of the heat generation rate or heat flux, and this local high gradient always can be considered as a kind of weak discontinuity. In solving such problems, a very small element size distribution in the region of high gradient is commonly needed as well as coupled with some special techniques such as curvilinear spectral overlay method. [Belytschko et al. (1990)] in continuous Galerkin method, and Ching et al. used the meshless Local Petrov-Galerkin (MLPG) method for transient thermomechanical response of a functionally graded composite heated by Gaussian laser beams [Ching and Chen (2006)].

Because of the discontinuous nature of the approximation function at the interface, it is possible to use fewer elements to capture the peak value of the heat flux in the temperature field with local high gradient. In the present research, we eliminate the penalization of the jump of the temperature at the interface in the region of local high gradient, and this relaxation makes the possible to capture the peak value of the heat flux a reality.

2.4.2 Problems with thermal contact resistance

Thermal contact resistance (TCR) arises in the contact region of two solids, because the two surfaces are not perfectly contact with each other, most of the heat passes through a limited number of actual contact spots, which means the real contact area is only a small fraction of the nominal or apparent area. Over the preceding decades, a lot of theoretical and experimental investigations have been performed to improve our knowledge of the TCR [Bahrami et al. (2006)]. Because of the existence of the TCR, the temperature jumps in the contact region while the heat flux remains continuous, and the TCR denoted by R is defined as the ratio of the temperature jump at the interface to the heat flux:

$$R = \frac{\Delta T}{q_n} \tag{37}$$

where ΔT denotes the temperature jump in the contact region and q_n denotes the heat flux normal to the interface.

In solving heat conduction problems with thermal contact resistance, Kanapady et al. presented the so-called local discontinuous Galerkin (LDG) finite element method [Kanapady et al. (2005)]. Blanford and Tauchert adopted linear interface elements to capture the temperature jump at the contact interface [Blandford and Tauchert (1985)]. Keppas et al. presented a boundary element procedure to treat two dimensional time dependent thermo-elastic contact problems with thermal contact resisitance [Keppas et al. (2008)]. In the present research, the penalization of the jump of the temperature on the imperfect contact interface is eliminated to capture the temperature jump, at the same time the interface numerical flux of the heat flux is substituted by the definition of the thermal contact resistance:

$$\mathbf{n}^e \cdot \hat{\mathbf{q}}^e = \frac{T^{eb} - T^e}{R} \tag{38}$$

This treatment may lead to a novel approach to capture the temperature jump at the imperfect contact interface.

2.4.3 Problems with thermoelastic coupling

Cylindrical contacts occur in many applications such as cylindrical tanks, space structures (heat pipes), power transmission lines, and nuclear fuel elements. So heat conduction problems through cylindrical contacts are very important, and a common phenomenon to understand in these problems is the thermoelastic coupling caused by TCR. We consider two dissimilar homogeneous and isotropic discs with initial gap $\delta_{gap} = b - a$ (see Fig. 3).

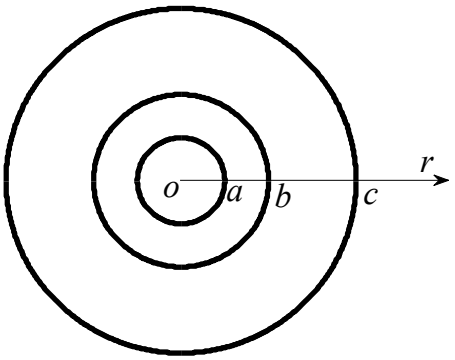

Figure 3: Illustration of two discs with initial gap δ_{gap}

We assume that heat is transferred from inner disc to outer disc. The two discs of different materials may be forced into contact with each other as a result of thermal expansion, so within the analysis there are two different solution states: gap-open state and gap-closed state which indicates the initial gap is still open and closed, respectively. In the first situation, although no contact has been made there still exists coupling between temperature field and TCR through radiation heat transfer. In the second situation, coupling phenomenon exists if an imperfect contact interface assumption is adopted: initial state of gap open makes the temperature of inner disc increases, and thermal expansion of the inner disc makes the gap closed which leads to the decrease of the TCR, and then the temperature jump at the interface decreases to make the gap open again. This results an on-off contact state caused by the coupling of temperature, TCR and interface stress shown in Fig. 4.

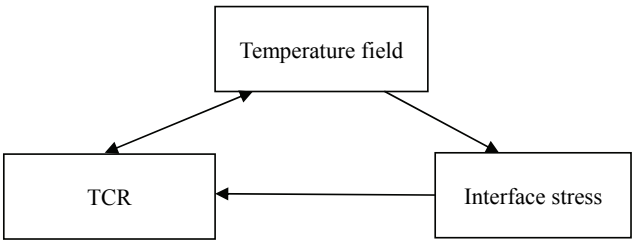

Figure 4: Illustration of the coupling between temperature field, interface stress and TCR

It is worth noting that traditionally coupling is just present in the case of finite deformations, and when dissipative processes like friction or plasticity have to be

considered. Because of the temperature-dependent nature of the material and the coupling of temperature, TCR and interface contact pressure, an iterative scheme is needed to solve the nonlinear equilibrium equations in Equation (36).

In order to avoid the over modification of the temperature vector and accelerate the convergence process, we adopt the relaxation technique in these circumstances, which means to use $\mathbf{T}+\alpha\cdot\Delta\mathbf{T}$ to update the current temperature vector instead of $\mathbf{T}+\Delta\mathbf{T}$, where α is the relaxation parameter and $0<\alpha<1$, and in the present research we adopt α=0.2.

3 Numerical examples

In this section, we consider some numerical examples in one and two dimensions to illustrate the properties and efficiencies of the DG finite element method.

3.1 Effect of stabilization parameter and numerical flux coefficients

Since the stabilization parameter and the numerical flux coefficients can greatly affect the stability and accuracy of the method, we consider the heat conduction problem in a one dimensional bar as the first numerical example to show how they work. The length of the bar is L=0.2 m, the isotropic thermal conductivity is k=46.3 $\mathrm{Wm^{-1}K^{-1}}$, and the area of the section is taken as A=0.001 $\mathrm{m^2}$. The heat generation rate is q_0=400 $\mathrm{kWm^{-3}}$. The left end of the bar has a specified temperature $T(0)$=350 K and the right end of the bar has a specified heat flux $g_0(L)$= 16 $\mathrm{kWm^{-2}}$. The bar is divided into 100 linear elements with the same size. The exact solution of the problem is given by:

$$T(x)=\frac{L^2}{k}\left(\frac{q_0}{2}\left(\frac{2x}{L}-\left(\frac{x}{L}\right)^2\right)+\frac{g_0 x}{L^2}\right)+T_1 \tag{39}$$

Fig. 5 and Fig. 6 show the variation of the local relative error of the temperature in the middle of the bar and the global error with the stabilization parameter respectively. Fig. 7 and Fig. 8 show the variation of the local relative error of the temperature in the middle of the bar and the global error with the temperature numerical flux coefficient α_T respectively, in which we assume that the heat flux numerical flux coefficient α_q is equal to the temperature numerical flux coefficient α_T. Here the global error is defined by the norm $\left\|\mathbf{T}^{DG}-\mathbf{T}^{exact}\right\|_2$, where $\mathbf{T}^{DG}$ is the node temperature vector calculated by the present DG finite element method, and $\mathbf{T}^{exact}$ is the corresponded exact node temperature vector.

It can be seen from Fig. 5 and Fig. 6 that whatever to consider the local relative error or the global error, the stabilization term is very necessary when using the Bassi-Rebay numerical flux. The proper range of the stabilization parameter is

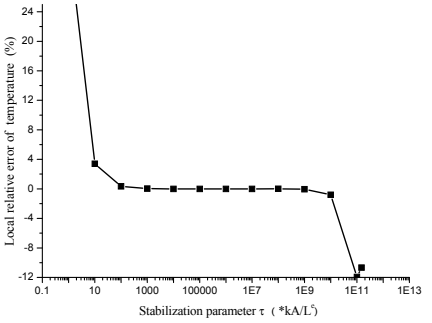

Figure 5: Variation of the local relative error of the temperature in the middle of the bar with the stabilization parameter τ

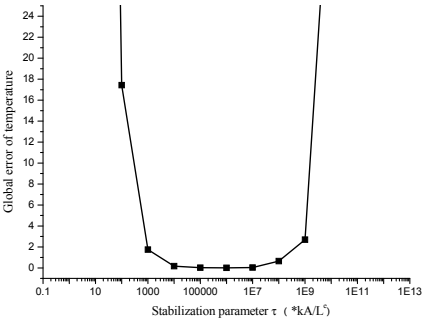

Figure 6: Variation of the global error of temperature with the stabilization parameter τ

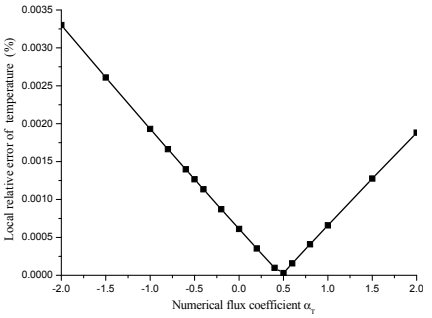

Figure 7: Variation of the local relative error of the temperature in the middle of the bar with the temperature numerical flux coefficient α_T

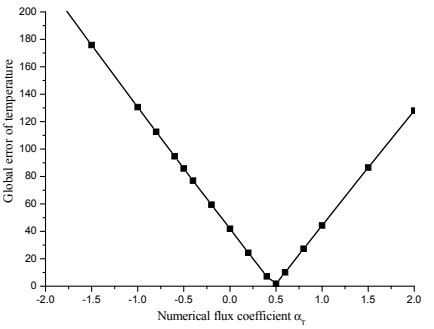

Figure 8: Variation of the global error of temperature with the temperature numerical flux coefficient α_T

10^4-10^8, any stabilization parameter out of this range may cause singularity to the stiffness matrix and leads to unstable or inaccuracy results. So in the following numerical examples, we adopt 10^7 as the stabilization parameter.

It can be seen from Fig. 7 and Fig. 8 that whatever to consider the local relative error or the global error, 0.5 is the best choice of the temperature numerical flux coefficient, that is to say, in the present problem numerical flux had better to be taken as the average of the value on the two segments of the interface. So in the following numerical examples, we adopt the Bassi-Rebay numerical flux with α_T $=\beta_T$ $=\alpha_q$ $=\beta_q$ $=0.5$.

3.2 Local high gradient temperature field

In the second example, we consider a one dimensional heat conduction problem with local high gradient. The length of the bar is L=6 m, and the isotropic thermal conductivity is k=1 $\mathrm{Wm^{-1}K^{-1}}$, and the boundary conditions are given by: $T(0)$=-tanh(3c) K and $T(L)$=tanh(3c) K, where c is a constant. The heat generation rate is given by:

$$q_0(x) = 2c^2 \mathrm{sech}^2(c(x-3)) \tanh(c(x-3)) \tag{40}$$

The exact solution the temperature field for this problem is [Belytschko and Lu (1992)]:

$$T = \tanh(c(x-3)) \tag{41}$$

Here we assume the constant c =40, and the bar is divided into 100 linear elements with the same size. Due to the sharp change of the heat generation at the middle of the bar, there exists local high gradient. Fig. 9 and Fig. 10 show the comparisons of the temperature distribution and heat flux distribution between the present DG finite element method and the exact results respectively, and Fig. 11 illustrates the computational efficiency of the present DG method in capturing the peak value of the heat flux.

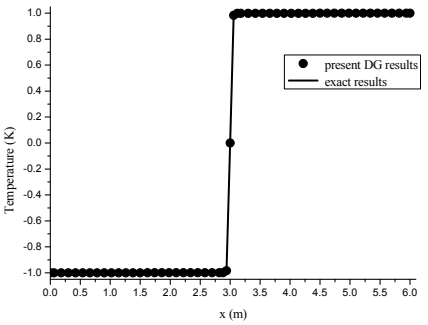

Figure 9: Comparison of the temperature distribution between the present DG results and exact results

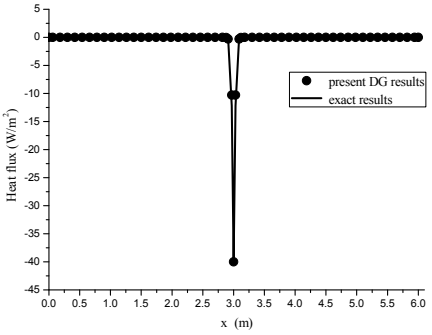

Figure 10: Comparison of the heat flux distribution between the present DG results and exact results

The comparisons in Fig. 9 and Fig. 10 reveal that the present DG results exactly match the analytical results. In fact, because of the discontinuous nature of the approximation function at the interface of the DG method, it is possible to use fewer

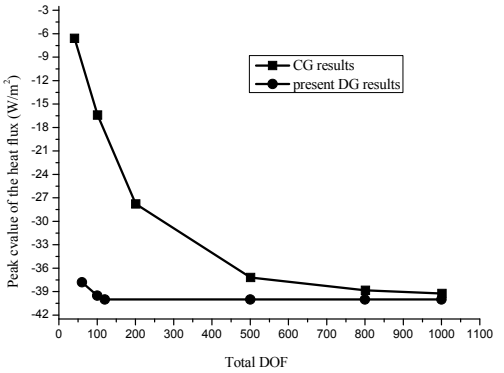

Figure 11: Comparison of the present DG results and the CG results on the variation of the peak value of the heat flux with the total DOF

elements to capture the peak value of the heat flux in the temperature field with local high gradient, and this advantage is illustrated in Fig. 11. From Fig. 11, it can be seen that the continuous Galerkin finite element method requires a very refined mesh (more than 1000 DOF) to capture the peak value of the heat flux. However, the present DG finite element method requires much less number of degrees of freedom (less than 150 DOF). The present DG method is even more efficient than the so-called local discontinuous Galerkin (LDG) finite element method proposed by Kanapady [Kanapady et al. (2005)] et al. which requires more than 200 DOF to capture the peak value of the heat flux.

So this example shows the validity and computational efficiency of the present DG method in modeling high gradient field.

3.3 Imperfect thermal contact of two bars

In the third example we consider the imperfect thermal contact of two bars to verify the validity and accuracy of the present DG method in capturing the temperature jump at the contact region caused by the thermal contact resistance. Geometry and description of the problem is given in Fig. 12. Two different values of interlayer thermal contact resistance are considered namely [Blandford and Tauchert (1985)]: R=0.34$\times 10^{-3}$ m^{2}KW^{-1} (a typical value for rolled steel plates subject to a compressive contact stress $\geq$25 MPa), R=3.80$\times 10^{-3}$ m^{2}KW^{-1} (a typical value for rough machined surfaces under zero compressive contact stress).

The exact results and the present DG results for the above cases are shown in Fig. 13(a) and Fig.13(b). The exact results were obtained using the formulation described in Appendix A. The DG finite element results were obtained using 5 linear

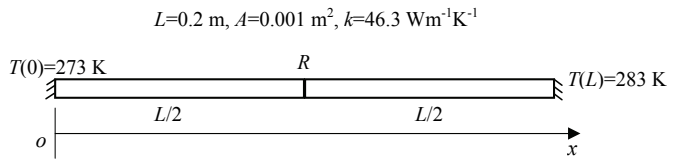

Figure 12: Geometry and description of the two imperfect thermal contact bars

elements in each bar. The temperature jump under different thermal contact resistance is shown in Fig. 14.

We can see from Fig. 13(a) and Fig.13(b) that the results of the present DG method are in excellent agreement with the exact results. Furthermore, thermal contact resistance increases the temperature magnitude within the left layer and decrease the temperature magnitude within the right layer whereas it has an opposite effect to the temperature gradients. Fig. 14 shows that with the increase of the thermal contact resistance, the temperature jump at the interface increases quickly, and the limit value of the temperature jump is 10 K.

This example shows the validity and accuracy of the present DG method in capturing the temperature jump in one dimensional heat conduction problem.

3.4 Fin and plate problem

In the fourth example, we consider the fin and plate problem that is typical in heat removal from electric devices. The goal of such structures is to keep the temperature of the plate as low as possible, and the key point is to keep the thermal contact resistance (TCR) between the fin and the plate as low as possible. Fig. 15 shows the discretization and the boundary conditions of the problem. We consider a segment containing only a fin, and due to the symmetry of the problem only one half of the geometry need to be analyzed. To increase heat dissipation on the upper side(BG) of a plate(OABG) subjected to heat flux from the bottom(OA), some fins(CDEF) are placed in contact with the plate. Here we neglect the gas contribution and radiation effects to the TCR and the TCR can be determined by Equation (A.9) in Appendix B. The main interesting input material and structure data of the problem are collected in Table 1.

Since the mechanical pressure between the fin and the plate is very important to the thermal contact resistance (see from Equation (A.9)), a series of numerical tests have been carried out varying the mechanical pressure applied in the contact zone. The temperature in some points of the structures, obtained by the present DG method, are compared with Wriggers' results shown in Fig. 16(a)-(d) and Fig. 17.

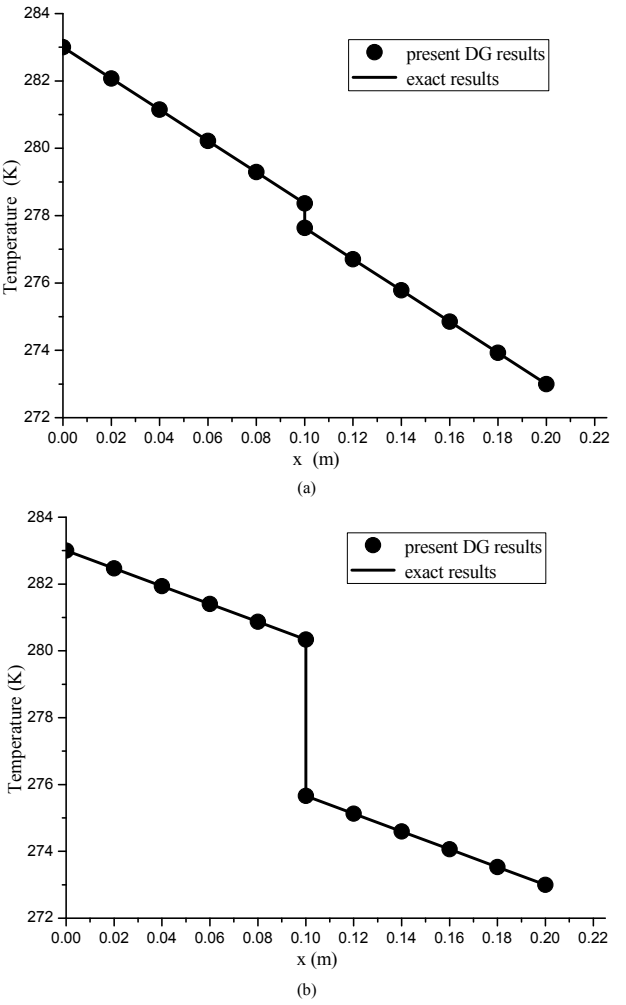

Figure 13: Comparison of the temperature distributions for two imperfect contact bars with different thermal contact resistance between the present DG results and exact results: (a) $R = 0.34 \times 10^{-3} m^2$K/W; (b) $R = 3.80 \times 10^{-3} m^2$K/W

It can be observed from Fig. 16(a)-(d) and Fig. 17 that the present DG results are in general close to those obtained by Wriggers et al. by using a two-node contact element [Wriggers and Zavarise (1993)], which show the validation of the present method in modeling two dimensional heat conduction problems with thermal contact resistance. Decreases of the temperature jump at the contact zone means that heat can be easily transferred from the plate to the fin, so Fig. 17 also shows that the

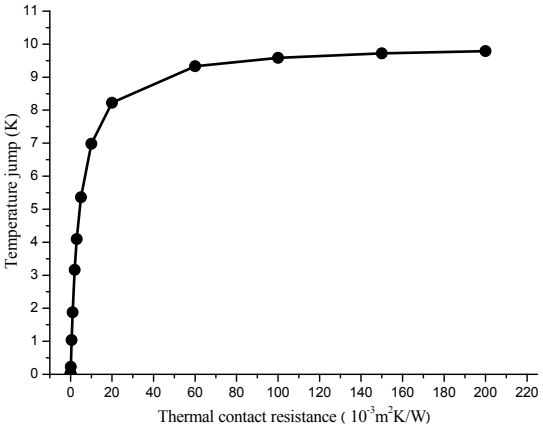

Figure 14: Variation of temperature jump with different thermal contact resistance

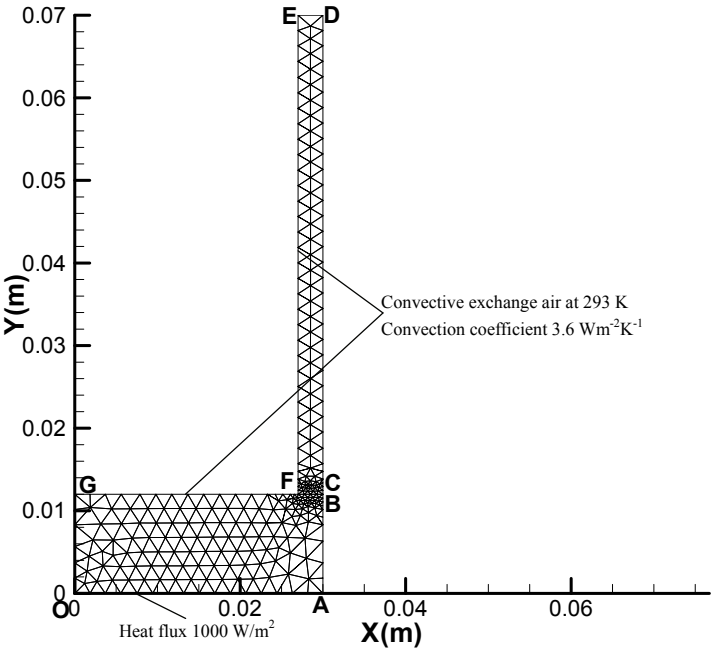

Figure 15: Fin and plate problem description

Table 1: Input parameters of material and structure

Characteristics	Values
RMS surface roughness	0.478×10^{-6} m
Mean absolute asperity slope	0.072
Experimental hardness parameters c_1	6.271 GPa
Experimental hardness parameters c_2	-0.229
Thermal conductivity	19.2 $\mathrm{Wm^{-1}K^{-1}}$

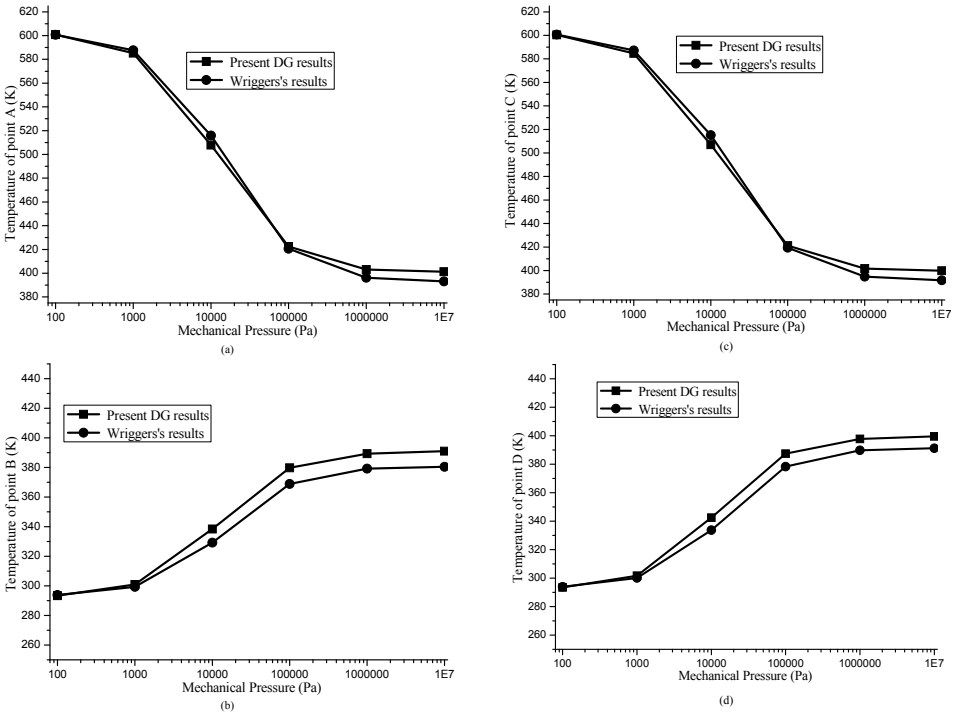

Figure 16: Comparisons of the variation of temperature at different points with the mechanical pressure at the contact zone between the present DG results and Wriggers' results [Wriggers and Zavarise (1993)]: (a)point A; (b)point B; (c)point C; (d)point D

thermal dissipation efficiency increases with the increase of the mechanical pressure. Since high mechanical pressure may bring the structure failure at the contact zone, it is very important in engineering practices that how to determine the balance point of the mechanical pressure with the considerations both of the structure safety and the thermal dissipation efficiency, and the present DG method provides

Table 2: Variations of inner material properties with temperature

Temperature (K)	Elastic modular E_i (GPa)	Thermal expansion coefficient α_i ($\times 10^{-6}$ 1/K, T_{ref}= 293 K)	Thermal conductivity k_i ($\mathrm{Wm^{-1}K^{-1}}$)	Yield Stress (MPa)
373	205	11.95	13.9	222.3
473	201	12.35	15.15	200.1
573	195	12.75	16.62	178.0
673	189	13.10	18.71	155.8
773	182	13.55	20.72	133.7
873	174	14.50	22.40	111.5
973	164	15.15	24.49	89.4
1073	155	15.70	27.00	67.2
1173	144	15.95	29.51	45.0
1273	132	16.20	31.60	22.9

Table 3: Variations of some interesting results with initial gaps

Initial gap (μm)	Interface temperature of inner disc (K)	Interface temperature of inner disc (K)	Temperature jump (K)	Contact stress (MPa)	Thermal contact resistance (m^2K/W)
0	637.1	607.2	29.9	125.7	9.92E-6
30	655.3	595.3	60.0	57.6	2.07E-5
40	672.0	584.2	87.8	36.7	3.15E-5
50	706.4	560.0	146.3	19.2	5.73E-5
60	773.0	508.4	264.6	7.842	1.29E-4
70	849.1	444.3	404.8	3.267	2.85 E-4
80	938.1	361.8	576.3	0.868	9.37E-4
90	996.6	303.5	693.1	0	0.02

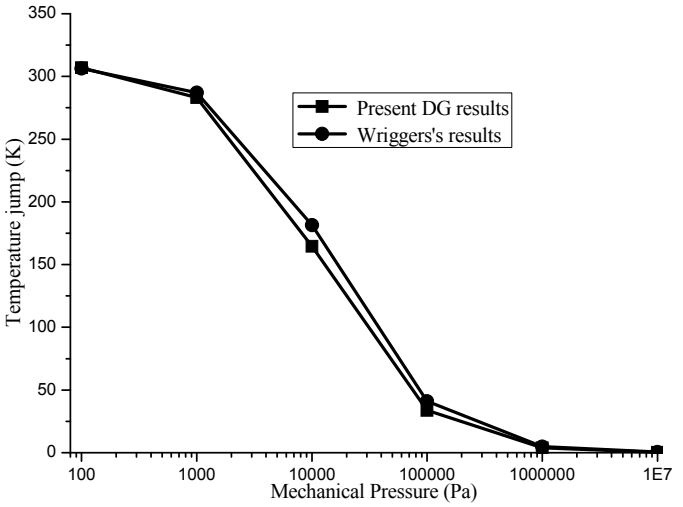

Figure 17: Comparisons of the variation of temperature jump at the contact zone with the mechanical pressure between the present DG results and Wriggers' results [Wriggers and Zavarise (1993)]

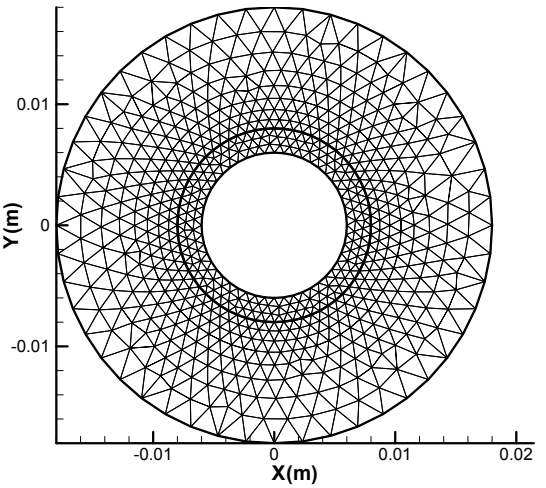

Figure 18: Discretization of the two discs

a noval approach to find this balance point efficiently and accurately.

3.5 Thermoelastic coupling of two discs caused by TCR

In this example, two dissimilar homogeneous and isotropic discs with imperfect thermal contact subjected to axially symmetric temperature field is investigated. Since there is initial gap between the two discs, the temperature jump, TCR and contact stress at the interface are changeable under different initial gaps. The purpose of this investigation is to show the efficiency of the DG method in dealing with the coupling problems of the temperature field, TCR and interface contact stress.

The following assumptions are adopted in the present research: thermal conductance (reciprocal of thermal contact resistance) is just caused by radiation which irrelevant to the width of the gap when there is no contact between the two discs, and it can be obtained from Appendix B; the thermal conductance is just caused by radiation and spots contact heat transfer which depends on the contact pressure when the two discs contact with each other, and the relationship between the temperature field and the contact pressure can be obtained from Appendix C; contact pressure is substituted by the yielding stress if the calculated contact pressure is larger than the yielding stress.

The inside and outside diameters of the inner disc are 0.012 m and 0.016 m respectively, and the inner and outside diameters of the outer disc are (0.016+δ_{gap}) m and 0.036 m respectively. δ_{gap} denotes the initial gap between the two discs. The specified temperature of the inner boundary of the inner disc is 1000 K, and the specified temperature of the outer boundary of the outer disc is 300 K. The properties for the outer material are assumed to be unchangeable: elastic modular E_o=51 GPa, Poisson ratio ν_o=0.33, thermal conductivity k_o=60 $\mathrm{Wm^{-1}K^{-1}}$, and thermal expansion coefficient α_o=0.46×10^{-6} 1/K. The properties of the inner material are considered to be temperature-dependent which are collected in Table 2 except the Poisson ratio is 0.3. Fig. 18 shows the discretization of the two discs.

The relaxation techniques described in subsection 2.4.3 is used to solve the present coupling problem. The convergence parameter η_T, residuum norm R_T, and unbalanced energy E_T are defined by:

$$\begin{aligned} \eta_T &= \frac{\|\Delta\mathbf{T}\|_2}{\|\mathbf{T}\|_2} \\ R_T &= \|\mathbf{F}-\mathbf{K}\mathbf{T}\|_2 \\ E_T &= (\mathbf{F}-\mathbf{K}\mathbf{T})^T\cdot\Delta\mathbf{T} \end{aligned} \tag{42}$$

where T is the current temperature vector, $\Delta\mathbf{T}$ is the increment of temperature vector, $\mathbf{F}$ is the current heat load vector, $\mathbf{K}$ is the current stiffness matrix. The conver-

gence criterion in the present study is:

$$\eta_T \leq \eta \tag{43}$$

where η is the temperature convergence tolerance.

Fig. 19 show the convergence process of the algorithm with different initial gaps.

We can see from Figs. 19(a)-(c) that, if the initial gap is small (e.g., less than 30 μm), the gap keeps closed during the iteration; if the initial gap is large (e.g., larger than 90 μm), the gap keeps open during the iteration, so the algorithm convergences quickly in these two cases. Otherwise, if the initial gap is moderate (e.g., equal to 60 μm), from the numerical point of view, an unstable solution is observed which the algorithm loops between the state of gap-closed and gap-open, unless the relaxation technique is adopted. Fig. 20 and Fig. 21 illustrate the temperature field and the radial temperature distribution with different initial gaps, respectively. Table 3 lists some interesting results such as interface temperature jump, contact stress and thermal contact resistance under different initial gap.

Interestingly, because the thermal expansion coefficient of the inner disc is larger than the outer disc and the efficient of spot heat transfer is greater than radiation heat transfer, small initial gap leads to a smaller temperature jump at the interface but a higher interface contact stress, and large initial gap leads to a larger temperature jump at the interface but a smaller interface contact stress as we can see from Fig. 21 and Table 3. In fact, both overmuch temperature jump and interface contact stress are dangerous to the structure, so there needs a match point to balance the temperature jump and the interface contact stress. The present DG method seems an impactful numerical technique in engineering design and analysis to find this match point. From our investigation, we also find that the present DG method has good capability in avoiding numerical instability to simulate the coupling of temperature, thermal contact resistance and interface contact stress.

4 Conclusions and discussions

The DG finite element method for heat conduction problems with local high gradient and TCR has been developed. The DG formulation is constructed by employing the stabilization term and the numerical flux term that allow apparently different formulations to be used. In the present research, we adopt the stabilization term defined by a penalization of the jump of the temperature at the interface and the Bassi-Rebay numerical flux. Numerical examples show that, generally, when stabilization parameter τ is assigned in the range $10^4<\tau<10^8$ and numerical flux coefficients $\alpha_T = \alpha_q$=0.5 is chosen, the best accuracy is achieved.

Because of the discontinuous nature of the approximation function at the interface,

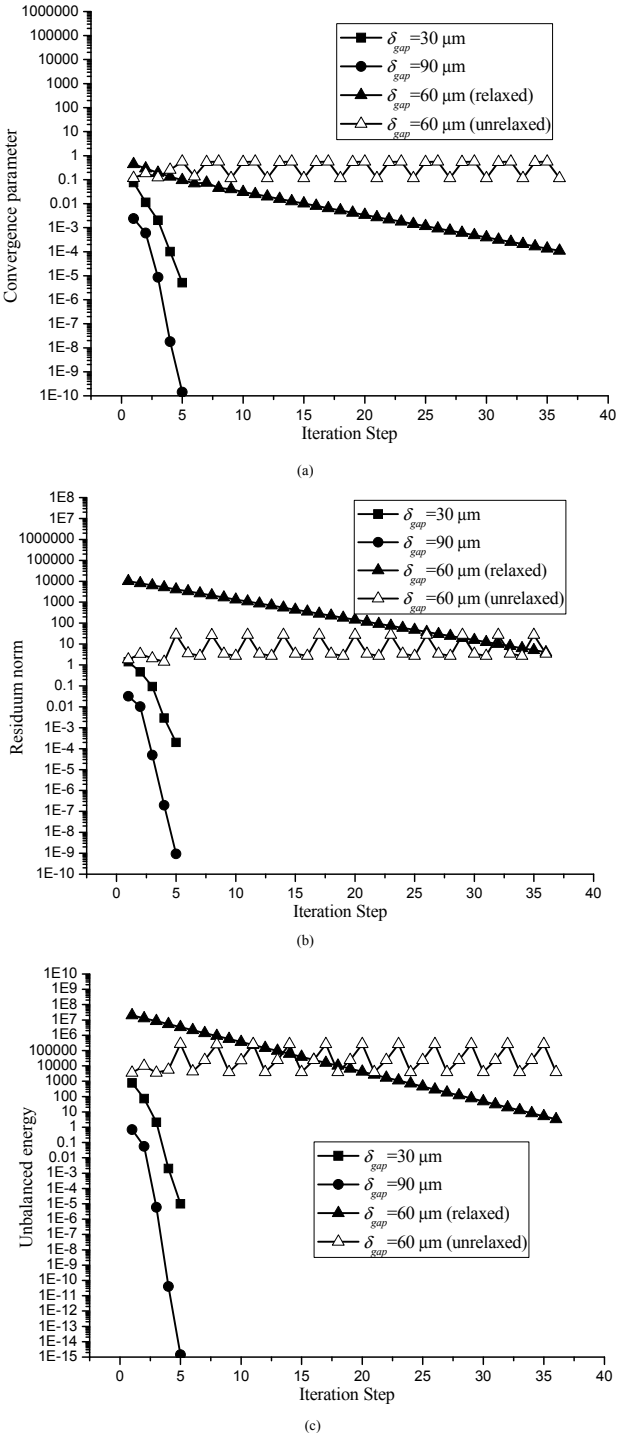

Figure 19: Convergence process of different error index with different initial gaps

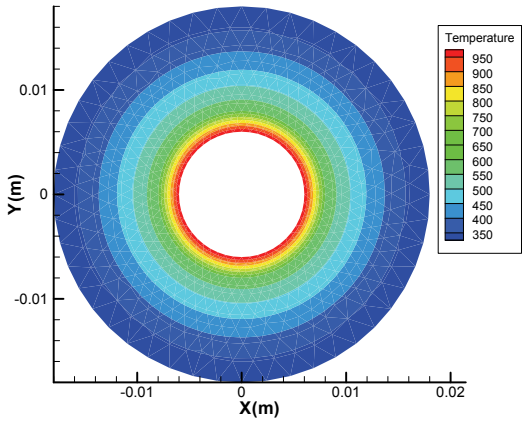

(a)

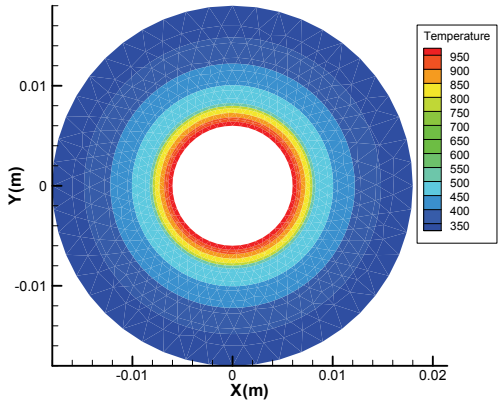

(b)

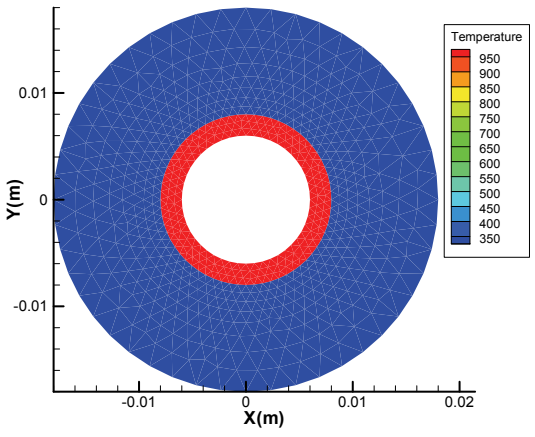

(c)

Figure 20: Temperature field with different initial gaps: (a) 30 μm, (b) 60 μm, (c) 90 μm

the present DG method can be conveniently applied to the problems involving local high gradient and thermal contact resistance, where the numerical flux is substituted by the definition of the thermal contact resistance. This treatment leads to a novel approach to capture the peak value of the heat flux in local high gradient field and the temperature jump at the imperfect contact interface. Numerical examples illustrate that the present DG method is not only high accurate in capturing the peak heat flux of local high gradient field and the temperature jump at the imperfect contact interface, but also has higher computational efficiency compared with traditional continuous Galerkin method and even the local discontinuous Galerkin method.

In solving the nonlinear coupling problem caused by thermal contact resistance, an iterative procedure and relaxation technique are suggested, which can efficienly aviod numerical instability, and the present DG method also presents an impactful numerical technique to find the match point to balance the temperature jump and the interface contact stress.

It should be mentioned that there are still a lot of work to do for DG method in further research. Firstly, the discontinuous nature of the shape functions introduces additional unknowns relative to the continuous Galerkin method, as we need to distinguish between values from different elements at the same node. Secondly, the implementation is more complicated than that of standard finite element procedures. This is evident in the treatment of the interfaces where information from neighbor elements is needed to construct the flux terms. However, the method is promising to efficient parallel implementation and adaptivity, which can reduce the effect of the increase of degrees of freedom. Moreover, as the high gradient and discontinuities are always located in some parts of the mesh, the coupled discontinuous/continuous Galerkin method is more preferable [Clint and Jennifer (2002)]. So future work aim at further enhancing the efficiency of the computations, especially in regions where the solution is smooth.

Acknowledgement: This research was supported by the National Natural Science Foundation of China, under Contract 10872104.

References

Aksoy, H. G.; Senocak, E. (2005): Modelling of functionally graded and layered materials With space-time discontinuous Galerkin method. *AIAA 2005-1924*, pp. 1-15.

Alberty, J.; Carstensen, C. (2002): Discontinuous Galerkin time discretization in elastoplasticity: motivation, numerical algorithms,and applications. *Computer Methods in Applied Mechanics and Engineering*, Vol. 191, pp. 4949-4968.

Arnold, D. N.; Brezzi, F.; Cockburn, B.; Marini, I. D. (2002): Unified analysis of discontinuous Galerkin methods for elliptic problems. *SIAM Journal of Numerical Analysis*, Vol. 39, pp. 1749-1779.

Bahrami, M.; Culham, J. R.; Yananovich, M. M.; Schneider, G. E. (2006): Review of thermal joint resistance models for nonconforming rough surfaces. *Applied Mechanics Reviews*, Vol. 59, pp. 1-12.

Bassi, F.; Rebay, S. (1997): A high-order accurate discontinuous finite element method for the numerical solution of the compressible Navier-Stokes equations. *Journal of Computational Physics*, Vol. 131, pp. 267-279.

Bassi, F.; Rebay, S. (1997): High-order accurate discontinuous finite element solution of 2D Euler equations. *Journal of Computational Physics*, Vol. 138, pp. 251-285.

Belytschko, T.; Fish, J.; Bayliss, A. (1990): The spectral overlay on finite elements for problems with high gradients. *Computer Methods in Applied Mechanics and Engineering*, Vol. 81, pp. 71-89.

Belytschko, T.; Lu, Y. Y. (1992): A curvilinear spectral overlay method for high gradient problems. *Computer Methods in Applied Mechanics and Engineering*, Vol. 95, pp. 383-396.

Blandford, G. E.; Tauchert, T. R. (1985): Thermoelastic analysis of layered structures with imperfect layer contact. *Computers & Structures*, Vol. 21, pp. 1283-1291.

Brezzi, F.; Cockburn, B.; Marini, L. D.; Süli, E. (2006): Stabilization mechanisms in discontinuous Galerkin finite element methods. *Computer Methods in Applied Mechanics and Engineering*, Vol. 195, pp. 3293-3310.

Celiker, F.; Cockburn, B.; Stolarski, H. k. (2006): Locking-free optimal discontinuous Galerkin methods for Timoshenko beams. *SIAM Journal of Numerical Analysis*, Vol. 44, pp. 2297-2325.

Chen, Z.; Gan, Y.; Chen, J. K. (2008): A coupled thermo-mechanicalmodel for simulating the material failure evolution due to localized heating. *CMES - Computer Modeling in Engineering and Sciences*, Vol. 26, pp. 123-137.

Chien, C. C.; Wu, T. Y. (2008): An improved predictor/multi-corrector algorithm for a time-discontinuous Galerkin finite element method in structural dynamics. *Computational Mechanics*, Vol. 25, pp. 430-437.

Ching, H. K.; Chen, J. K. (2006): Thermomechanical analysis of functionally graded composites under laser heating by the MLPG method. *CMES - Computer Modeling in Engineering and Sciences*, Vol. 13, pp. 199-218.

Clint, D.; Jennifer, P. (2002): Coupling of continuous and discontinuous Galerkin

methods for transport problems. *Computer Methods in Applied Mechanics and Engineering*, Vol. 191, pp. 3213-3231.

Cockburn, B. (2003): Discontinuous Galerkin methods. *ZAMM Zeitschrift für Angewandte Mathematik und Mechanik*, Vol. 83, pp. 731-754.

Cockburn, B.; Kanschat, G.; Schotzau, D. (2005): The local discontinuous Galerkin method for linearized incompressible fluid flow: a review. *Computers and Fluids*, Vol. 34, pp. 491-506.

Cockburn, B.; Karniadakis, G. E.; Shu, C.-W. (2000): The development of discontinuous Galerkin methods. *Discontinuous Galerkin methods: Theory, Computation and Applications*, Berlin, Springer.

Dolean, V.; Fol, H.; Lanteri, S.; Perrussel, R. (2008): Solution of the time-harmonic Maxwell equations using discontinuous Galerkin methods. *Journal of Computational and Applied Mathematics*, Vol. 218, pp. 435-445.

Du, Q. H.; Yu, S. W.; Yao, Z. H. (1986): *Theory of Elasticity*. Beijing, Science Press.

Engel, G.; Garikipati, K.; Hughes, T. J. R.; Larson, M. G.; Mazzei, L.; Taylor, R. L. (2002): Continuous/discontinuous finite element approximations of fourth-order elliptic problems in structural and continuum mechanics with applications to thin beams and plates, and strain gradient elasticity. *Computer Methods in Applied Mechanics and Engineering*, Vol. 191, pp. 3669-3750.

Eyck, A. T.; Lew, A. (2006): Discontinuous Galerkin methods for non-linear elasticity. *International Journal for Numerical Methods in Engineering*, Vol. 67, pp. 1204-1243.

Güzey, S.; Cockburn, B.; Stolarski, H. K. (2007): The embedded discontinuous Galerkin method: Application to linear shell problems. *International Journal for Numerical Methods in Engineering*, Vol. 70, pp. 757-790.

Güzey, S.; Stolarski, H. K.; Cockburn, B.; Tamma, K. K. (2006): Design and development of a discontinuous Galerkin methods for shells. *Computer Methods in Applied Mechanics and Engineering*, Vol. 195, pp. 3528-3548.

Hansbo, P.; Larson, M. G. (2002): Discontinuous Galerkin methods for incompressible and nearly incompressible elasticity by Nitsche's method. *Computer Methods in Applied Mechanics and Engineering*, Vol. 191, pp. 1895-1908.

Jain, A.; Kanapady, R.; Tamma, K. K. (2006): Local Discontinuous Galerkin Formulations for parabolic problems Involving imperfect contact surfaces. *AIAA-2006-0590*, pp. 1-11.

Kanapady, R.; Jain, A.; Tamma, K. K.; Siddharth, S. (2005): Local Discontinuous Galerkin Formulations for Heat Conduction Problems Involving High Gradi-

ents and Imperfect Contact Surfaces. *AIAA-2005-0762*, pp. 1-9.

Keppas, L. K.; Giannopoulos, G. I.; Anifantis, N. K. (2008): Transient coupled thermoelastic contact problems incorporating thermal resistance: a BEM approach. *CMES - Computer Modeling in Engineering and Sciences*, Vol. 25, pp. 181-196.

Khalmanova, D. K.; Costanzo, F. (2008): A space-time discontinuous Galerkin finite element method for fully coupled linear thermo-elasto-dynamic problems with strain and heat flux discontinuities. *Computer Methods in Applied Mechanics and Engineering*, Vol. 197, pp. 1323-1342.

Li, Q.; Shen, S.; Han, Z. D.; Atluri, S. N. (2003): Application of meshless local petrov-galerkin (MLPG) to problems with singularities, and material discontinuities, in 3-D elasticity *CMES - Computer Modeling in Engineering and Sciences*, Vol. 4, pp. 571-585

Li, X. D.; Wiberg, N. E. (1998): Implementation and adaptivity of a space-time finite element method for structural dynamics. *Computer Methods in Applied Mechanics and Engineering*, Vol. 156, pp. 211-229.

Madhusudana, C. V.; Fletcher, L. S. (1981): Gas conductance contribution to contact heat transfer *AIAA 81-1163*, pp. 1-8.

Masuda, S.; Noguchi, H. (2006): Analysis of structure with material interface by meshfree method. *CMES - Computer Modeling in Engineering and Sciences*, Vol. 11, pp. 131-143.

Noels, L.; Radovitzky, R. (2006): A general discontinuous Galerkin method for finite hyperelasticity. Formulation and numerical applications. *International Journal for Numerical Methods in Engineering*, Vol. 68, pp. 64-97.

Reed, W. H.; Hill, T. R. (1973): Triangular mesh methods for the neutron transport equation. *Technical Report LA-UR-73-479*, Los Alamos Scientific Laboratory.

Sherwin, S. J.; Kirby, R. M.; Peiro, J.; Taylor, R. L.; Zienkiewicz, O. C. (2006): On 2D elliptic discontinuous Galerkin methods. *International Journal for Numerical Methods in Engineering*, Vol. 65, pp. 762-784.

Song, S.; Yovanovich, M. M. (1987): Explicit relative contact pressure expressions: dependance upon surface roughness parameters and Vickers micro-hardness coefficients. *AIAA-87-0152*.

Warburton, T.; Karniadakis, G. (1999): A discontinuous Galerkin method fot the viscous MHD equations. *Journal of Computational Physics*, Vol. 152, pp. 1-34.

Wriggers, P.; Zavarise, G. (1993): Thermomechanical contact–a rigorous but simple numerical approach. *Computers and Structures*, Vol. 46, pp. 47-53.

Zienkiewicz, O. C.; Taylor, R. L.; Sherwin, S. J.; Peiro, J. (2003): On discontinuous Galerkin methods. *International Journal for Numerical Methods in*

Engineering, Vol. 58, pp. 1119-1148.

Appendix A Exact solution of the temperature jump in two imperfect contact bars

In this appendix we give the exact solution of the temperature jump in two imperfect contact bars. Each bar is of length $L/2$, and the isotropic thermal conductivity is k, the interlayer thermal contact resistance is R. The boundary conditions are taken as: $T(0)= T_1$ and $T(L)= T_2$. We adopt "+" and "-" to denote the left side and right side of the contact interface.

The heat flux in the left bar and right bar can be calculated as:

$$\begin{aligned} q_R^+ &= k\frac{T_1 - T_R^+}{L_R} \\ q_R^- &= k\frac{T_R^- - T_2}{L - L_R} \end{aligned} \tag{A.44}$$

The heat flux is continuous at the interface, so we have:

$$q_R = q_R^- = q_R^+ \tag{A.45}$$

Then the thermal contact resistance can be calculated as:

$$R = \frac{\Delta T}{q_R} = \frac{T_R^+ - T_R^-}{q_R} \tag{A.46}$$

With Equation (A.1) and Equation (A.3) we can obtain:

$$\begin{aligned} T_R^+ &= T_1 + \frac{L_R}{L + kR}(T_2 - T_1) \\ T_R^- &= T_2 + \frac{L - L_R}{L + kR}(T_1 - T_2) \end{aligned} \tag{A.47}$$

And the temperature jump is:

$$\Delta T = T_R^+ - T_R^- = \frac{kR}{L + kR}(T_1 - T_2) \tag{A.48}$$

The heat flux in the bar can be calculated by:

$$q = k\frac{T_1 - T_2}{L + kR} \tag{A.49}$$

As can be seen from (A.6) , thermal contact resistance makes the effective length of the bar has an increment of kR.

Appendix B Thermal contact resistance model

The purpose of the present research is not to develop a new thermal contact resistance model, but to show the efficiency of the DG method in capturing the temperature jump in the contact zone for a given value of the thermal contact resistance. So in this appendix, we just give the thermal contact resistance model from the former researchers.

As we know, the heat exchange takes place by conduction through the contact spots, conduction through the gas contained in the cavities and radiation between cavity surfaces, and conduction through the interstitial materials if they are used in the interface. This leads to the following relationship for the thermal contact resistance R:

$$\begin{aligned} \frac{1}{R} &= \frac{1}{R_{spot}} + \frac{1}{R_{gas}} + \frac{1}{R_{radiation}} \text{ without interstitial material} \\ \frac{1}{R} &= \frac{1}{R_{spot}} + \frac{1}{R_{intmat}} \text{ with interstitial material} \end{aligned} \tag{A.50}$$

or in terms of the heat conductance h:

$$\begin{aligned} h &= h_{spot} + h_{gas} + h_{radiation} \text{ without interstitial material} \\ h &= h_{spot} + h_{intmat} \text{ with interstitial material} \end{aligned} \tag{A.51}$$

There have been several comprehensive reviews in thermal contact resistance modeling and experiment. Song and Yovanovich suggested that the heat conductance caused by spots contact heat transfer can be calculated as. [Song and Yovanovich (1987)]:

$$h_{spot} = \frac{1.25k^*\bar{m}}{\sigma}\left(\frac{p_N}{c_1}\left(1.6177\frac{10^6\sigma}{\bar{m}}\right)^{-c_2}\right)^{\frac{0.95}{1+0.0711c_2}} \tag{A.52}$$

Where $k^* = 2k_1k_2/(k_1+k_2)$ is the mean thermal conductivity of the two contact materials, $\bar{m}$ is the mean absolute asperity slope, σ is RMS surface roughness, p_N is the apparent mechanical pressure, and c_1,c_2 are experimental hardness parameters determined with micro hardness tests.

The contribution of the gas that contained in the micro-cavities to the heat conductance can be calculated as [Madhusudana and Fletcher (1981)]:

$$h_{gas} = \frac{k_{gas}}{d+g_1+g_2} \tag{A.53}$$

Where k_{gas} is the gas conductivity, and d is the effective height of the cavity which corresponding to the mean plane distance:

$$d = 1.363\sigma\sqrt{-\ln\left(5.589\frac{p_N}{H_e}\right)} \tag{A.54}$$

Where H_e is the micro hardness distribution. Terms g_1 and g_2 are introduced to reproduce the nonlinear surface effect and the temperature surface discontinuity, and can be calculated as:

$$g_1 + g_2 = \left(\frac{2-\alpha_1}{\alpha_1} + \frac{2-\alpha_2}{\alpha_2}\right)\frac{2\gamma}{\gamma+1}\frac{1}{\Pr}\Lambda_0\frac{T}{T_0}\frac{p_{g0}}{p_g} \tag{A.55}$$

Where α_1 and α_2 are experimental coefficients related to the two contact surfaces respectively. $\gamma = c_p/c_v$ indicates the specific heat ratio, where c_p and c_v are specific heat capacity at constant pressure and constant volume respectively. Λ_0 is the mean free path calculated at reference temperature T_0 and reference gas pressure p_{g0}. T and p_g are the current temperature and reference gas pressure respectively. Pr is the Prandtl number defined by:

$$\Pr = \frac{\mu c_p}{k_{gas}} \tag{A.56}$$

Where μ is the viscosity coefficient of the gas.

Heat transfer by radiation works in a vacuum as well as in a gas medium circumstance. The basic relation for the heat flux due to radiation is given in terms of the Stefan-Boltzmann law:

$$q = c_{em}c_{SB}F_{12}\left(T_1^4 - T_2^4\right) \tag{A.57}$$

Where c_{em} is the surface emissivity, c_{SB} is Stefan-Boltzmann constant, F_{12} is the mutual radiation factor of the two surfaces. In the present research, we assume that c_{SB}= 5.67×10^{-8} $\mathrm{Wm^{-2}K^{-4}}$, c_{em}=0.8, and F_{12} =1.

Then the heat conductance caused by radiation can be calculated as:

$$h_{rad} = \frac{q}{T_1 - T_2} = c_{em}c_{SB}\left(T_1^2 + T_2^2\right)(T_1 + T_2) \tag{A.58}$$

Often the radiation effects between the surfaces of the micro-cavities can be neglect, because the low temperature greatly reduces this effect. However the radiation effect might be important to regularize the jump in the thermal resistance between status gap open and status gap closed as we can see in section 3.5 or when the interface temperature is high.

We can easily obtain the heat conductance caused by interstitial material contact heat transfer by substituting the thermal conductivity k^* in Equation (A.9) with the thermal conductivity k^*_{intmat}:

$$h_{intmat} = \frac{1.25 k^*_{intmat} \bar{m}}{\sigma} \left(\frac{p_N}{c_1} \left(1.6177 \frac{10^6 \sigma}{\bar{m}} \right)^{-c_2} \right)^{\frac{0.95}{1+0.0711 c_2}} \tag{A.59}$$

Appendix C Relationship of the axially symmetric temperature field and interface contact stress of two contact discs

In this section, the relationship of the axially symmetric temperature field and interface contact stress of two contact discs is given. The radial displacement of the plane stress disc subjected to axially symmetric temperature field with inside diameters $2r_1$ and outside diameters $2r_2$ are given by [Du et al. (1986)]:

$$u_r = \frac{\alpha}{r} \left((1+\nu) \int_{r_1}^{r} (T - T_0) \, r \mathrm{d}r + \frac{(1-\nu) r^2 + (1+\nu) r_1^2}{r_2^2 - r_1^2} \int_{r_1}^{r_2} (T - T_0) \, r \mathrm{d}r \right) \tag{A.60}$$

If it is a plane strain problem, then we just need to substitute α, E, ν in Equation (A.17) with α^*, E^*, ν^* which are defined by:

$$\alpha^* = \alpha (1+\nu), E^* = \frac{E}{1-\nu^2}, \quad \nu^* = \frac{\nu}{1-\nu} \tag{A.61}$$

Here we consider two discs with cylindrical contact that are subjected to axially symmetric temperature field. The inside and outside diameters of the inner disc are a and b respectively, and the inside and outside diameters of the outer disc are b and c respectively. The material parameters of the inner material and outer material are denoted by subscript i and o, respectively. We assume that the thermal expansion coefficient of the inner material is larger than the outer material. The radial displacement of an annual disc with inner and outer pressure is given by [Du et al. (1986)]:

$$u_r(r) = \frac{1}{E\left(r_o^2 - r_i^2\right)} \left(\left(p_i r_i^2 - p_o r_o^2 \right) (1-\nu) \, r + r_i^2 r_o^2 \left(p_i - p_o \right) (1+\nu) \frac{1}{r} \right) \tag{A.62}$$

According to Equation (A.19), the interface pressure p_N on inner and outer disc caused negative and positive displacement respectively and are given by:

$$\begin{aligned} u_i^p &= \frac{p_N b^2}{E_i (b^2 - a^2)} \left(\frac{(1+\nu_i) a^2}{b} + (1-\nu_i) b \right) \\ u_o^p &= \frac{p_N b^2}{E_o (c^2 - b^2)} \left(\frac{(1+\nu_o) c^2}{b} + (1-\nu_o) b \right) \end{aligned} \tag{A.63}$$

Considering that the interference stress p_N is cause by thses two displacements u_i^p and u_o^p in (A.20), we have:

$$p_N = \frac{u_i^p + u_o^p}{R\left(\frac{c^2+b^2}{E_o(c^2-b^2)} + \frac{a^2+b^2}{E_i(b^2-a^2)} + \frac{\nu_o}{E_o} - \frac{\nu_i}{E_i}\right)} \tag{A.64}$$

According to Equation (A.17), the interface displacements of inner and outer disc with temperature field $T(r)$ are given by:

$$\begin{aligned} u_b^i &= \frac{2\alpha_i b}{b^2-a^2}\int_a^b (T-T_0)\, r\mathrm{d}r \\ u_b^o &= \frac{2\alpha_o b}{c^2-b^2}\int_b^c (T-T_0)\, r\mathrm{d}r \end{aligned} \tag{A.65}$$

The compatible condition of the displacement is:

$$u_b^i + u_b^o = u_i^p + u_o^p \tag{A.66}$$

Using Equations (A.21)(A.22)(A.23), the relationship of the temperature field and interface pressure can be written as:

$$p_N = \frac{u_b^i + u_b^o}{b\left(\frac{c^2+b^2}{E_o(c^2-b^2)} + \frac{a^2+b^2}{E_i(b^2-a^2)} + \frac{\nu_o}{E_o} - \frac{\nu_i}{E_i}\right)} \tag{A.67}$$